

TiO₂-based sensor arrays modeled with nonlinear regression analysis for simultaneously determining CO and O₂ concentrations at high temperatures

Marla L. Frank^a, Matthew D. Fulkerson^b, Bruce R. Patton^b, Prabir K. Dutta^{a,*}

^aDepartment of Chemistry, Center for Industrial Sensors and Measurements (CISM), The Ohio State University,
120 West 18th Avenue, Columbus, OH 43210, USA

^bDepartment of Physics, Center for Industrial Sensors and Measurements (CISM), The Ohio State University,
174 West 18th Avenue, Columbus, OH 43210, USA

Received 3 June 2002; received in revised form 30 July 2002; accepted 20 August 2002

Abstract

Responses of TiO₂-based sensor arrays were analyzed using kernel ridge regression modeling to determine the concentrations of CO and O₂ in gas mixtures at 873 K. Two variations of a two-sensor combination were studied. In each array, a La₂O₃-doped TiO₂ sensor was used, whereas the second sensor in the array was a CuO–La₂O₃-doped TiO₂ sensor, doped with different levels of copper. In sensor array I, 2 wt.% CuO was used, while 8 wt.% CuO was used in the second. Sensor array I was used to demonstrate the kernel ridge regression methodology. The concept of orthogonality of sensors was developed, which is a quantitative measure of how well the sensor array can discriminate between the two gases of interest. This model was then used to extract the concentrations of CO and O₂ in a gas mixture over ranges of 2–10% O₂ and 250–1000 ppm CO using the second sensor array. Prediction ability was found to be reasonable over certain concentration ranges and was determined by the orthogonality of the sensor responses.

© 2002 Elsevier Science B.V. All rights reserved.

Keywords: Anatase; Kernel regression; Support vector machines; Combustion exhaust monitoring; Emissions monitoring

1. Introduction

High temperature combustion processes require the complete conversion of hydrocarbons to H₂O and CO₂ for maximum efficiency [1]. These processes are done with a controlled amount of fuel and air to maximize output and minimize emissions [1]. Emission abatement strategies are an active area of research [2] and are closely tied to the combustion process. Incomplete combustion can lead to the formation of CO and unreacted hydrocarbons, and lower efficiency of the process. Therefore, the monitoring of CO and O₂ gas during combustion processes should be useful in determining the efficiency of combustion. Sensors for determining CO and O₂ individually are well studied. For example, metal oxide sensors, based on oxides like SnO₂, are extensively used for monitoring CO at temperatures below 673 K [3,4]. In a resistive sensor such as SnO₂, oxygen species from the gas phase chemisorb to the surface of the SnO₂ grains, trapping electrons at this surface to form a

depletion layer. When two grains are in contact with one another, the presence of this depletion layer causes an energy barrier for electrons to move from one grain to the next, known as the Schottky barrier [5]. A reducing gas such as CO reacts with the surface oxygen species and causes electrons to be released back to the bulk, decreasing the resistance of the sensor and is the basis for sensing of CO [5]. If the sensor is operating under ambient conditions, where the oxygen content remains relatively stable at 21%, then such a sensor should respond selectively to a reducing gas. However, in a dynamic combustion environment, the oxygen content of the background gas is lower than ambient and constantly changing, thus altering the concentration of chemisorbed oxygen species, which in turn changes the baseline resistance of the sensor and will make it impossible to determine the concentration of the reducing gas. Potentiometric O₂ sensors that work by generating a Nernstian potential across a solid electrolyte also show interference towards CO because its oxidation will lead to a mixed potential [6–8]. Thus, determining CO and O₂ in a dynamic combustion environment by simply employing conventional sensors is not a workable strategy. The high temperatures of

* Corresponding author. Tel.: +1-6142924532; fax: +1-6146885402.
E-mail address: dutta.1@osu.edu (P.K. Dutta).

a combustion environment also demand sensors that can operate at temperatures greater than 673 K.

Previously, our group has examined TiO₂-based sensors capable of selective detection of CO in the presence of methane at temperatures of 773 K and above in 5% O₂ with background of N₂ [9–11]. Although capable of operating at high temperatures, metal oxide sensors based on TiO₂ have the same problems as outlined above for SnO₂, since they are sensitive to changes in oxygen content of the background gas.

Recently, considerable attention has focused on the use of multiple sensors coupled with pattern recognition techniques to determine the components of a mixture of several gases that interfere with each other [12–15]. Pattern recognition techniques such as principal components analysis and artificial neural networks have been used to differentiate gases in a mixture [12–15]. These techniques, although widely used, have several shortcomings. Principal components analysis is generally limited in its ability to describe nonlinear sensor behavior and to predict component gas concentrations because of its linear nature. While artificial neural networks have been used to predict different concentrations of gases in a mixture, large training sets, which involve considerable time and cost for data collection, are typically required for reliable results.

The goal of the present study was to detect CO and O₂ in changing backgrounds using a dual set of TiO₂-based sensors, which respond to both gases. A pattern recognition modeling algorithm based on kernel ridge regression has been developed to predict gas concentrations. In order to generate sensors for use in the array, La₂O₃ and CuO were used as dopants. La₂O₃ stabilizes the anatase phase of the TiO₂ and limits grain growth. Our previous studies with CuO had shown that the sensitivity of CO over CH₄ was enhanced, and the transformation of n-type anatase to p-type rutile was promoted by CuO [9,10]. The set of sensors chosen for this study consisted of a CuO/La₂O₃-doped TiO₂ sensor and a La₂O₃-doped TiO₂ sensor. For the CuO/La₂O₃-doped TiO₂ sensor, two levels of CuO were used to change the sensor properties, 2% CuO/10% La₂O₃-doped TiO₂ and 8% CuO/10% La₂O₃-doped TiO₂. The sensor array consisting of La₂O₃-doped TiO₂ and 2% CuO/10% La₂O₃-doped TiO₂ was used to set up the model. The 8% CuO/10% La₂O₃-doped TiO₂ sensor, in combination with the 10% La₂O₃-doped TiO₂ sensor, was used to test prediction ability of CO and O₂ in a mixture. The kernel ridge regression technique was used to model the sensor data, estimate the extent of information available from each sensor array (the concept of orthogonality) and predict the concentration of gases in a mixture.

2. Experimental

2.1. Sample preparation

Sensor materials for sensor array I were made by mechanical mixing of commercial metal oxide powders. Commercial anatase (99.9%, Aldrich), La₂O₃ (Aldrich) and CuO

(Aldrich) were weighed to achieve 10 wt.% La₂O₃-anatase (AL) and 2 wt.% CuO–10 wt.% La₂O₃-anatase (2% CuO-AL), ball-milled and calcined at 1073 K for 6 h. This procedure has been outlined previously [9]. For sensor array II, the La₂O₃-CuO was fabricated using the chemisorption-hydrolysis method [16]. In this case, commercial anatase and La₂O₃ were ball-milled and calcined as above. A solution of [Cu(NH₃)₄]²⁺ was prepared by addition of NH₄OH to Cu(NO₃)₂·3H₂O solution until a pH of 9 was achieved. The 10% La₂O₃-TiO₂ powder was then added and the slurry was stirred for 20 min. After stirring, the copper complex was hydrolyzed and deposited onto the 10% La₂O₃-TiO₂ by slow dilution of the slurry in an ice bath. The solid was then filtered, washed with water and dried overnight at 393 K. This dried solid was calcined for 6 h at 1073 K. The amount of CuO deposited onto the 10% La₂O₃-TiO₂ is estimated to be 8% (8% CuO-AL), according to the amount of starting materials used. A paste of suitable consistency for screenprinting was achieved by mixing each powder with appropriate amounts of organic vehicle, solvent and dispersant. A thin layer of paste was screenprinted onto alumina substrates with interdigitated gold electrodes. After screenprinting, each sensor was heated at 473 K for 2 h to remove organic material and calcined at 1073 K for 6 h.

2.2. Electrical measurements and data analysis

Sensing measurements were done at 873 K. Both oxygen and CO concentrations were varied with nitrogen gas making up the balance. Oxygen concentrations of 2, 5 and 10% were used. CO gas concentrations ranged from 250 to 1000 ppm. The setup used for sensing measurements has been previously described [11]. This setup has been modified to accommodate up to three sensors at a time. The sensors were placed in a quartz tube inside a tube furnace. The test gas mixtures were passed through the tube with a total flow rate of 100 ml/min. Concentrations of gases in the various mixtures were controlled by digital mass flow controllers. A Hewlett-Packard Data Acquisition/Switch Unit (HP 34970A) interfaced with a desktop computer was used for data acquisition. Sensor samples were equilibrated for 2 h at the initial oxygen concentration to allow the baseline resistance to stabilize. Sensors were equilibrated for 20–30 min upon subsequent changes in oxygen concentrations and 10–15 min between each CO concentration until the baseline resistance restabilized. CO measurements were made in stepwise fashion.

All data analysis algorithms used to model the sensor data were developed using Matlab 5.3.

3. Results

3.1. Basis of the regression model

In order to quantify gases in a multicomponent mixture, it is necessary to model the sensor response functions. For a

given sensor, the measured response, y_j , can be described by a sensor response function:

$$y_j = f_j(\vec{x}). \tag{1}$$

It is necessary to have as many sensors as gases that produce a sensor response. For the determination of CO and O₂ in a mixture, which was the focus of this study, a two-sensor array was used. A multivariate nonlinear regression technique known as kernel ridge regression was used to model the experimental data and provide the basis for predictions of gas concentrations in mixtures [17].

3.1.1. Kernel ridge regression

Given a set of data points, $\{(\vec{x}_i, y_i)\}$, where \vec{x}_i is a point in the domain of gas concentrations and y_i is the corresponding measured value of the sensor response, we seek a sensor response function, $y = f(\vec{x})$, of the form

$$f(\vec{x}) = \sum_n w_n \phi_n(\vec{x}). \tag{2}$$

The functions $\{\phi_n(\vec{x})\}$ are a family of nonlinear basis functions to be used in regression and $\{w_n\}$ are the weights found through the regression analysis. If these weights were found directly, as in ordinary linear regression, the computational time necessary would rapidly increase with the number of basis functions. Therefore, only a limited number of basis functions could be used. Kernel ridge regression, however, allows use of a large (or infinite) number of basis functions. In this case, the optimal weights are expressed as a linear combination of basis functions:

$$w_n = \sum_i \alpha_i \phi_n(\vec{x}_i). \tag{3}$$

Substitution of Eq. (3) into Eq. (2) leads to a dual representation of $f(\vec{x})$:

$$f(\vec{x}) = \sum_i \alpha_i K(\vec{x}_i, \vec{x}). \tag{4}$$

The kernel function K is defined by

$$K(\vec{x}, \vec{x}') = \sum_i \phi_n(\vec{x}) \phi_n(\vec{x}'). \tag{5}$$

This allows one to solve for dual variables $\{\alpha_i\}$ instead of finding the primal weights $\{w_n\}$ directly. Thus, the size of the problem scales with the number of data points rather than the number of basis functions, and one is able to avoid an arbitrary restriction of the number of basis functions. There are several choices of basis functions. It was found that for the sensors examined in this study, best results were obtained with exponential functions, which have features that are similar to the sensor responses.

3.1.2. Determining the composition of a gas mixture

The computational steps taken in predicting the composition of a mixture using the exponential function basis set as an example include:

- (i) Determining the kernel function for the set of all decaying exponential functions, $\{\phi_{\vec{b}}(\vec{x}) = e^{-\vec{b}(\vec{a} + \vec{x})} : \vec{b} > \vec{0}\}$. Note that the basis functions can be written $\phi_{\vec{b}}(\vec{x}) = e^{-\vec{b}\vec{a}} e^{-\vec{b}\vec{x}}$. The components of the vector \vec{a} are positive constants (~ 0.1 or 1) that introduce a cutoff for \vec{b} , since the amplitude $e^{-\vec{b}\vec{a}}$ becomes exponentially small as \vec{b} increases.

The function defined in Eq. (5) is given by the reciprocal kernel:

$$\begin{aligned} K(\vec{x}, \vec{x}') &= \int_0^\infty db_1 \int_0^\infty db_2 \phi_{\vec{b}}(\vec{x}) \phi_{\vec{b}}(\vec{x}') \\ &+ \int_0^\infty db_1 \phi_{(b_1, 0)}(\vec{x}) \phi_{(b_1, 0)}(\vec{x}') \\ &+ \int_0^\infty db_2 \phi_{(0, b_2)}(\vec{x}) \phi_{(0, b_2)}(\vec{x}') + 1 \\ &= \prod_{v=1,2} \left\{ \frac{1}{(2a_v + x_v + x'_v)} + 1 \right\}. \end{aligned} \tag{6}$$

The product runs over all gas types involved in the sensor response (i.e. $v = 1, 2$ is for CO, O₂).

- (ii) The dual variables, which determine the fit, are given by

$$\alpha_i = \sum_j (\mathbf{K} + \lambda \mathbf{1})_{ij}^{-1} y_j, \tag{7}$$

where the elements of the matrix \mathbf{K} are the kernel function evaluated at the known gas composition data points:

$$(\mathbf{K})_{ij} \equiv K(\vec{x}_i, \vec{x}_j). \tag{8}$$

- (iii) The fit to the sensor response is constructed from the dual variables using Eq. (4).
- (iv) Steps (i), (ii), and (iii) are repeated for each sensor in the array and the function $f(x)$ is generated for each case.
- (v) Sensor measurements are taken upon exposing the array to an unknown mixture of the gases. Setting the measured response of each sensor in the array to the corresponding fitted response function results in the set of Eq. (1).
- (vi) The set of nonlinear Eq. (1) is then solved for the unknown gas composition \vec{x} . There are many software packages available for accomplishing this task. Here we have used the Matlab 5.3 function *fsolve*.

3.2. Model development: sensor array I

The two sensors used in sensor array I were a La₂O₃-doped TiO₂ sensor (AL) and a 2% CuO-AL sensor. This array was exposed to mixtures of 250–1000 ppm CO at O₂ concentrations of 2, 5 and 10%. Fig. 1 (a) and (b) show the responses of the two sensors for the given gas mixtures.

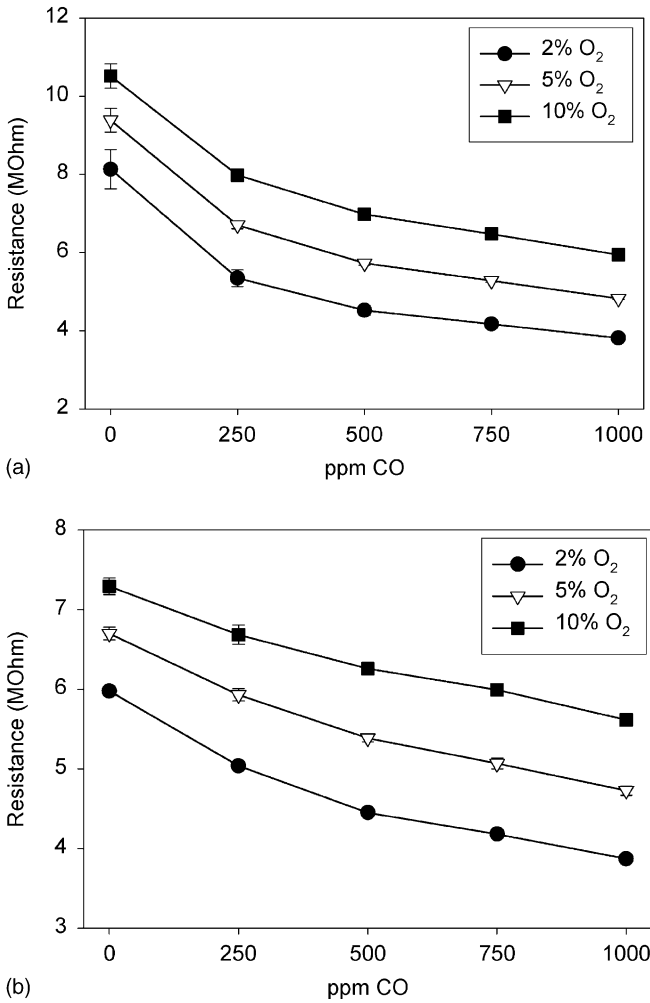


Fig. 1. Absolute responses of (a) AL sensor and (b) 2% CuO-AL sensor to 250–1000 ppm CO and 2–10% O₂ (sensor array I).

All measurements were performed in a nitrogen balance at 873 K and responses are represented as resistances in MΩ. For each gas mixture composition, the average of three data points is shown, with the standard deviation represented by vertical error bars. The reproducibility of the sensor responses was good, as shown by the small standard deviations, as long as sensor was maintained at high temperature. Significant changes in the baseline resistance of the sensors was observed if the sensors were subjected to heating and cooling cycles, probably due to mechanical changes in the film that alter bonding with the electrode-lined substrate. The relative resistances however, remained within a narrow range (15%). Nevertheless, since the regression model developed in this study uses absolute resistances of the sensors, it was necessary to keep the sensors continuously heated over the testing period (weeks).

Fig. 1 shows that the resistances of both sensors decreased with increasing CO and decreasing O₂, as would be expected for an n-type semiconductor. This data was used to model the sensor responses. Two kernel functions were chosen. The first was based on a family of exponential functions which

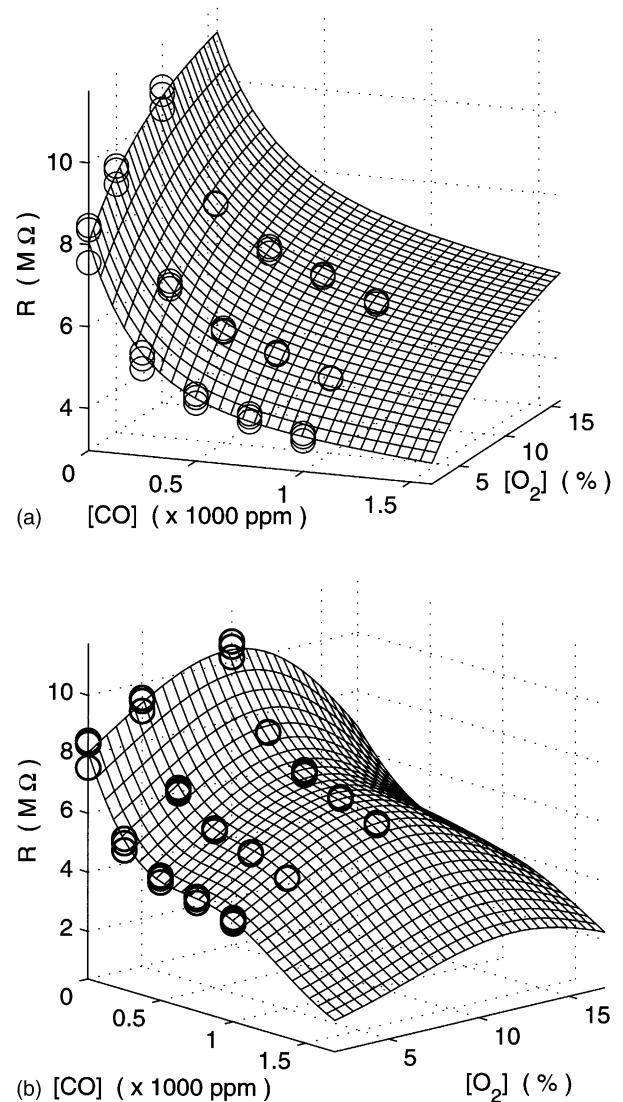


Fig. 2. Kernel ridge regression fit of AL sensor response using (a) reciprocal kernel and (b) Gaussian kernel.

leads to the *reciprocal* kernel shown in Eq. (6). The second was a Gaussian kernel function shown in Eq. (9):

$$K(\vec{x}, \vec{x}') = e^{-|\vec{x} - \vec{x}'|^2 / \sigma^2}. \quad (9)$$

Fig. 2 compares the fit to the AL sensor data using both kernel functions. Though both response functions go through the data points, the *reciprocal* kernel does a much better job of fitting the observed responses, especially beyond the data points. The Gaussian kernel tends to produce a more wavy fit and does not generalize well beyond the observed data points. Thus, the exponentials provide a better choice of basis functions, and all sensor responses were modeled using the *reciprocal* kernel.

By using the functions that model the sensor response, it is possible to define the ranges over which the sensor array can make predictions for unknown concentrations. There are two related ways to visualize the prediction ability. First is to

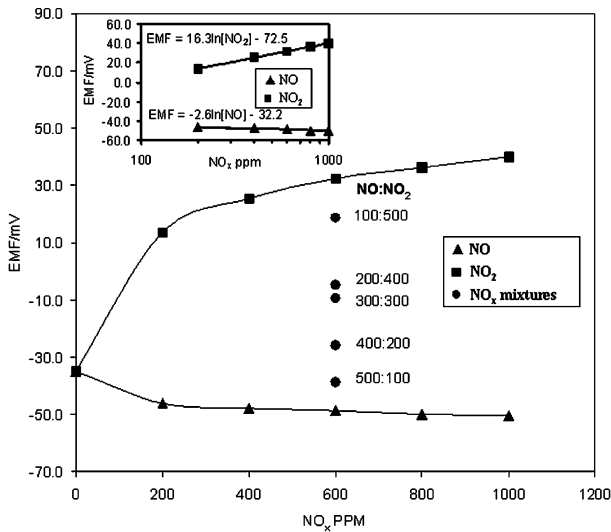


Fig. 3. Contour plots of AL and 2% CuO-AL modeled responses (sensor array I) overlain on one another, where each contour represents a line of constant resistance of the sensor (solid line: 2% CuO-AL; dashed line: AL).

plot constant resistance contour plots for both sensors using the modeled functions. Each contour line corresponds to the constant resistance of the sensor. When the contours for two sensors are overlain on one another, as shown in Fig. 3 for sensor array I, the concentrations of gases in a mixture can be found from the positions of intersection of the contours. The most unique information about composition is obtained from contours that intersect at right angles. If the contours are parallel, without a well-defined intersection point, then an unambiguous determination of concentration cannot be made. The regions where the contours for AL and 2% CuO-AL consistently intersect were for concentrations of CO <400 ppm and O₂ concentrations of 0–10%. The contours become more parallel as the CO concentration increases for all O₂ levels.

A related, but more quantitative, way to express the ability of the sensor array to predict gas compositions is to determine an orthogonality parameter for the entire composition space. The responses, $f_1(\vec{x})$ and $f_2(\vec{x})$, of two perfectly orthogonal sensors would satisfy

$$\vec{\nabla}f_1(\vec{x}) \perp \vec{\nabla}f_2(\vec{x}), \quad (10)$$

where $\vec{\nabla}f(\vec{x})$ is the gradient of the function at \vec{x} . In practice, it is enough if the gradients of the sensor responses are not nearly parallel. For the case of two sensors, a quantitative measure of orthogonality is the area of the parallelogram spanned by the vectors $\vec{\nabla}f_1(\vec{x})$ and $\vec{\nabla}f_2(\vec{x})$. This area is given by

$$A = |\vec{\nabla}f_1(\vec{x})| |\vec{\nabla}f_2(\vec{x})| \sin(\theta). \quad (11)$$

Along with the area, the angle θ also provides a measure of the orthogonality. Large gradients provide better predictions given that any measurement has an associated error. Fig. 4

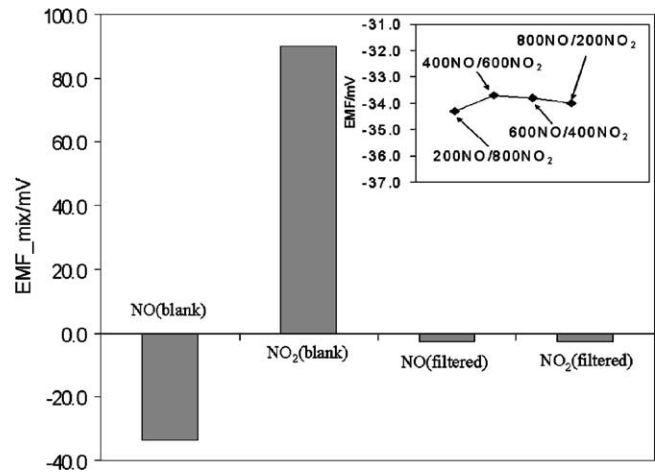


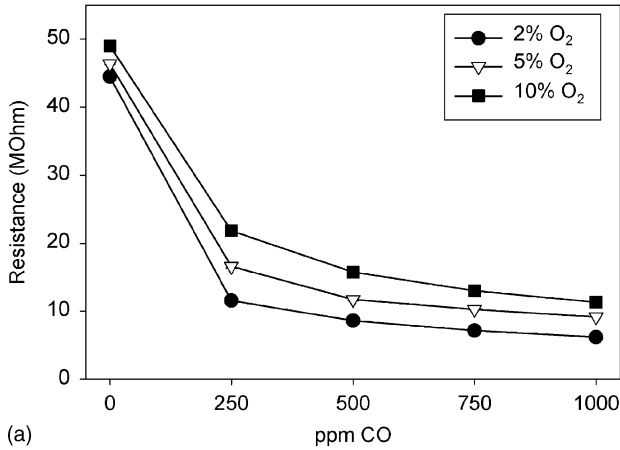
Fig. 4. Orthogonality index plot (using area) for AL and 2% CuO-AL sensors (sensor array I).

shows the plot of the orthogonality parameter for sensor array I and clearly demonstrates that the orthogonality peaks at CO concentrations <200 ppm and O₂ concentrations <2%. The sensors exhibit very little orthogonality for concentrations of CO >500 ppm at all O₂ concentrations. The information content of the contour plots (Fig. 3) and orthogonality (Fig. 4) are comparable, with Fig. 4 providing a more quantitative measure. Based on these plots, the prediction ability of sensor array I should be restricted to CO concentrations <400 ppm for O₂ ranges of 0–10%, with the best predictions coming at the lower end of these concentrations.

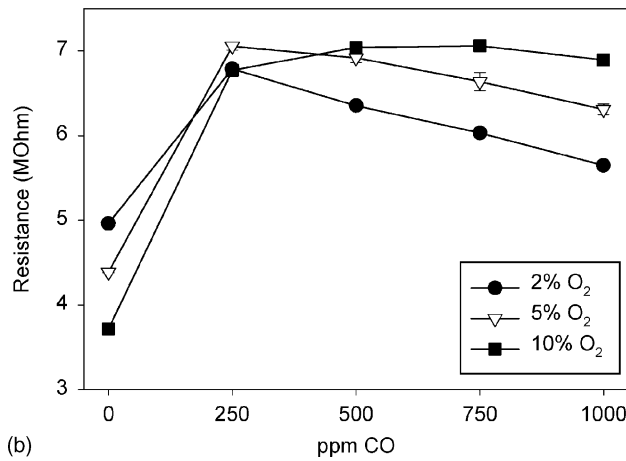
3.3. Prediction of gas compositions: sensor array II

A second combination of sensors was evaluated for prediction of gas concentrations using the kernel ridge regression model. The two sensors in array II were an AL sensor and a CuO-doped sensor with CuO concentration of 8% using a solution-based doping method [16]. XRD of the calcined 8% CuO-AL powder showed partial transformation of the starting anatase to the rutile phase. Fig. 5(a) and (b) shows the responses of the AL and 8% CuO-AL sensors to 0–1000 ppm CO in the presence of 2, 5 and 10% O₂.

It should be noted that though data in Figs. 1(a) and 5(a) are from sensors with similar compositions, there is quite a variation in their response. This is because the sensors were not prepared with identical thickness and also the thermal cycling of the sensors were very different. These differences in the sensor response are not going to be relevant in this study, since the sensor response within each array was very reproducible. However, it does point out the difficulty of fabrication of similar sensors, even from the same composition. The response of the AL sensor towards CO and O₂ is typical of an n-type semiconducting oxide. On the other hand, the resistance of the 8% CuO-AL sensor increases with increasing O₂ concentrations indicative of p-type behavior,



(a)



(b)

Fig. 5. Absolute responses of AL sensor (a) and 8% CuO-AL sensor (b) to 250–1000 ppm CO and 2–10% O₂ (sensor array II).

which is also evident upon addition of 250 ppm CO. At higher CO concentrations, the sensor exhibits n-type behavior. Thus, at lower concentrations of CO, the behavior of the sensor is like a p-type semiconductor, which changes to n-type at high CO concentrations. Kernel ridge regression was used to model the array II data. Fig. 6 shows the function that was generated for the data from the 8% CuO-AL sensor, using the reciprocal kernel function. The function does an excellent job of fitting the experimental data, and the transition from p- to n-type behavior around 250 ppm CO over the O₂ range is clearly evident.

The data for the AL sensor was also fitted using the same kernel function (similar to Fig. 2(a)).

The function for the AL and 8% CuO-AL sensors was used to generate the contour plot shown in Fig. 7. The contours tend to intersect at concentrations of CO between 100 and 400 ppm over the complete range of O₂ concentration. Fig. 8 shows the orthogonality plot, represented as the angle between the gradients and shows clearly that the orthogonality of the sensors is peaked somewhat sharply around 200 ppm CO. Based on the contour and orthogonality plots, the prediction would be that CO concentrations

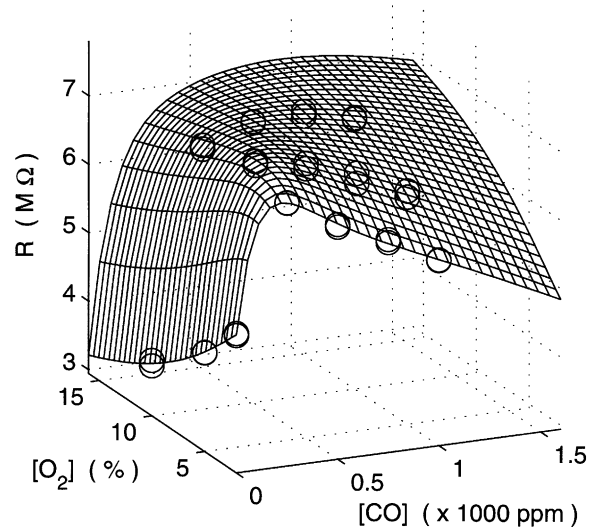


Fig. 6. Kernel ridge regression fit of 8% CuO-AL sensor response using reciprocal kernel.

between 100 and 400 ppm and O₂ concentrations over 0–10% can be made with certainty. In order to verify these predictions, we examined a series of gas mixtures of CO and O₂ and measured the corresponding resistance. Using the regression functions calculated for the AL and 8% CuO-AL from the data shown in Fig. 5, the resistances were used to predict the gas concentrations of the mixtures, as outlined in Section 3.1.2. Table 1 shows the gas compositions and the corresponding resistances of the sensor array II. Table 2 compares the actual and predicted concentration (**best predictions in bold**). It is clear that the best predictions are for the 250 ppm CO at all O₂ concentrations, as would be expected from the contour and orthogonality plots. In the regions where the orthogonality is poor (>400 ppm CO), predictions for both CO and O₂ are very poor.

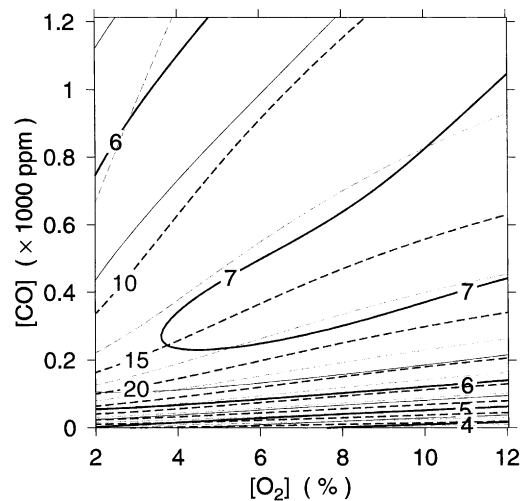


Fig. 7. Contour plots of AL and 8% CuO-AL modeled responses (sensor array II) overlain on one another, where each contour represents a line of constant resistance of the sensor (solid line: 8% CuO-AL; dashed line: AL).

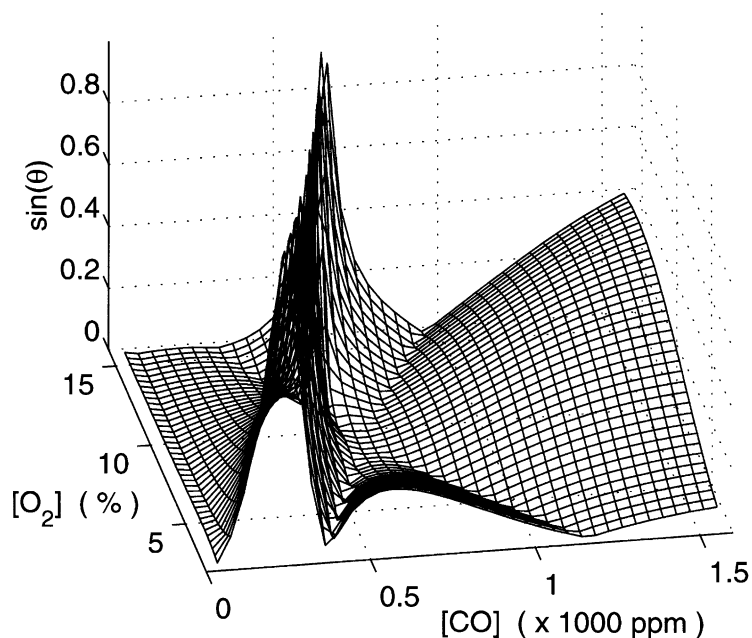


Fig. 8. Orthogonality index plot (using $\sin \theta$) for AL and 8% CuO-AL sensors (sensor array II).

Table 1

Absolute resistances of AL and 8% CuO-AL sensors (sensor array II) upon exposure to test mixtures of CO and O₂

Actual % O ₂	Actual [CO] (ppm)	AL resistance (MΩ)	8% CuO-AL resistance (MΩ)
3	250	12.58	6.89
3	350	11.89	6.76
3	600	9.43	6.58
3	800	8.21	6.35
3	900	7.80	6.17
4	250	14.24	6.91
4	350	11.40	6.83
4	600	10.34	6.79
4	800	9.19	6.64
4	900	7.96	6.26
8	250	20.38	7.01
8	700	10.69	6.81
8	900	11.50	6.91
9	250	21.06	6.92
9	700	11.25	6.86
9	900	10.15	6.82

Table 2

Comparison of actual and predicted values of CO and O₂ in test mixtures (using sensor array II)

Actual % O ₂	Predicted % O ₂	Actual [CO] (ppm)	Predicted [CO] (ppm)
3	2.59	250	259.18
3	1.81	350	228.55
3	2.87	600	524.21
3	1.86	800	494.94
3	2.36	900	701.7
4	2.78	250	215.95
4	2.38	350	294.95
4	2.73	600	404.26
4	2.03	800	407.02
4	2.04	900	580.68
8	8.57	250	254.64
8	11.44	700	1270.39
8	10.24	900	1005.11
9	8.79	250	241.56
9	3.36	700	405.15
9	16.88	900	1775.03

4. Discussion

4.1. Factors that control orthogonality

When choosing sensors for the array, it is essential for each sensor to provide independent information concerning the composition of a mixture of gases. Prediction ability is strongly dependent on the orthogonality of the modeled sensor response functions. It is therefore important to understand what features in the sensor array lead to orthogonality for the gases of interest. For sensor array I, though the

behavior of AL and 2% CuO-AL sensors is in general similar, careful inspection of Fig. 1 shows that the rate of decrease of resistance with concentrations of CO is different, particularly at low CO concentrations. This is because addition of Cu to TiO₂ leads to a flattening of the response, and the reasons for this behavior are currently being investigated.

By increasing the copper loading to 8% CuO and changing the method of doping, the sensing mechanism is altered, and TiO₂ acts as a p-type semiconductor. The doping of lower valent ions into TiO₂ leads to creation of holes,

which negate the electron carriers arising from oxygen stoichiometry [10,18]. At sufficient loadings, p-type behavior is manifested. However, with the loading we chose, there was a competition between p- and n-type pathways and, more significantly, the p to n transition for this sensor occurred at a certain concentration of CO (250 ppm in this case), and was fairly independent of O₂ concentrations. Since two sensors would be maximally orthogonal if each sensor was only sensitive to one of the gas components, orthogonality is achieved in the 200–400 ppm CO concentration region because of the insensitivity to oxygen.

4.2. Limitations of predictability

In the present study, a two-sensor array was chosen even though there were three gases in the sensing environment, CO, O₂, CO₂. This is because CO₂ does not give a response, as the gas cannot be further oxidized. However, if CO₂ produced a sensor response, then a third sensor would have to be included in the array, even if our interest is restricted to CO and O₂ only. Thus, the number of sensors in the array needs to match the number of gas species that produce independent sensor responses, immaterial of the number of specific gases of interest. For monitoring combustion processes, which is the goal of this program, this would require an additional hydrocarbon and NO_x sensor and is being investigated by our group [19,20]. For particular gases of interest, it may be necessary to have several combinations of sensors to cover the range of gas compositions of interest. For example, sensor array I with 2% CuO does provide a high degree of orthogonality for O₂ and CO at very low levels of both CO and O₂, whereas, sensor array II with 8% CuO has high orthogonality at low levels of CO for a wide range of O₂ concentrations. The error in prediction can be minimized by developing sensor materials that produce a higher degree of orthogonality between sensors, as well as by improving the accuracy and precision of the sensor responses.

4.3. Features of the kernel regression model

With a relatively small amount of test data, kernel ridge regression is able to determine the amount of unique information provided by each sensor in a set. The choice of basis functions is, however, very important. The exponential basis functions did a better job of fitting the sensor responses since the sensors produced monotonic responses that eventually saturated at high CO concentrations for a fixed O₂ level. Since a range of concentrations satisfy Eq. (1) within experimental error, there is an inherent uncertainty of the predictions. Added to this uncertainty is the effect that as the orthogonality of the sensors at the particular composition gets smaller, the error gets larger. Thus, the precision of the predictions will improve with reductions in experimental error and increasing orthogonality of the sensors. The orthogonality is a measure of independence in the information being provided by the sensors. This concept can be

readily extended to more than two sensors. For a three-sensor array, the volume of the parallelepiped spanned by the three gradient vectors is a measure of the orthogonality. For the kernel ridge regression model to predict unknown gas compositions, it is necessary to have the same number of sensors in the array as the gas components, if the sensors respond to each of these gases.

5. Conclusions

It has been demonstrated in this study that several TiO₂-based sensors combined with kernel ridge regression can be used to predict the concentrations of CO and O₂ in a mixture of these gases at high temperatures. By doping TiO₂ with La₂O₃ and different levels of CuO, the sensors can be modified to provide orthogonal information over specific gas concentration ranges. It has also been shown that kernel ridge regression is a useful technique for screening the redundancy of sensors for use in an array. While this paper demonstrates this regression technique for a set of two sensors and two gases, it can easily be expanded to more sensors for gas mixtures containing multiple components.

Acknowledgements

This work was supported by a NASA Graduate Student Research program grant to Marla L. Frank and grants from the Glennan Microsystems Initiative. We also acknowledge the help of Mr. Tim Henthorne for making the sensor array holders.

References

- [1] N. Docquier, S. Candel, Combustion control and sensors: a review, *Prog. Energy Combust. Sci.* 28 (2002) 107–150.
- [2] R.G. Herman, J.W. Sale, H.G. Stenger Jr., C.E. Lyman, J.E. Agogliatti, Y. Cai, B. Ramachandran, S. Choi, Monitoring aging and deactivation of emission abatement catalysts for selective catalytic reduction of NO_x, *Topics Catal.* 18 (2002) 251–257.
- [3] G.B. Barbi, J.P. Santos, P. Serrini, P.N. Gibson, M.C. Horriolo, L. Manes, Ultrafine grain-size tin-oxide films for carbon monoxide monitoring in urban environments, *Sens. Actuators B* 24/25 (1995) 559–563.
- [4] G. Tournier, C. Pijolat, R. Lalauze, B. Patissier, Selective detection of CO and CH₄ with gas sensors using SnO₂ doped with palladium, *Sens. Actuators B* 26/27 (1995) 24–28.
- [5] P.T. Moseley, J.O.W. Norris, D.E. Williams (Eds.), *Techniques and Mechanisms in Gas Sensing*, Adam Hilger, Bristol, 1991, pp. 109–138.
- [6] W.J. Fleming, Physical principles governing nonideal behavior of the zirconia oxygen sensor, *J. Electrochem. Soc.* 124 (1977) 21–28.
- [7] R. Kocache, *Gas sensors*, *Sens. Rev.* 14 (1994) 8–12.
- [8] Z.Y. Can, H. Narita, J. Mizusaki, H. Tagawa, Detection of carbon monoxide by using zirconia oxygen sensor, *Solid State Ionics* 79 (1995) 344–348.
- [9] N.O. Savage, S.A. Akbar, P.K. Dutta, Titanium dioxide based high temperature carbon monoxide selective sensor, *Sens. Actuators B* 72 (2001) 239–248.

- [10] N. Savage, B. Chwieroth, A. Ginwalla, B.R. Patton, S.A. Akbar, P.K. Dutta, Composite n–p semiconducting titanium oxides as gas sensors, *Sens. Actuators B* 79 (2001) 17–27.
- [11] P.K. Dutta, A. Ginwalla, B.D. Hogg, B.R. Patton, B. Chwieroth, Z. Liang, P. Gouma, M. Mills, S. Akbar, Interaction of carbon monoxide with anatase surfaces at high temperatures: optimization of a carbon monoxide sensor, *J. Phys. Chem. B* 103 (1999) 4412–4422.
- [12] K. Brudzewski, S. Osowski, Gas analysis system composed of a solid-state sensor array and hybrid neural network structure, *Sens. Actuators B* 55 (1999) 38–46.
- [13] G. Huyberegts, P. Szcwoka, J. Roggen, B.W. Licznanski, Simultaneous quantification of carbon monoxide and methane in humid air using a sensor array and an artificial neural network, *Sens. Actuators B* 45 (1997) 123–130.
- [14] J. Getino, L. Ares, J.I. Robla, M.C. Horrillo, I. Sayago, M.J. Fernandez, J. Rodrigo, J. Gutierrez, Environmental applications of gas sensor arrays: combustion atmospheres and contaminated soils, *Sens. Actuators B* 59 (1999) 249–254.
- [15] H.-K. Hong, C.H. Kwon, S.-R. Kim, D.H. Yun, K. Lee, Y.K. Sung, Portable electronic nose system with gas sensor array and artificial neural network, *Sens. Actuators B* 66 (2000) 49–52.
- [16] F. Bocuzzi, A. Chiorino, G. Martra, M. Gargano, N. Ravasio, B. Carrozzini, Preparation, characterization and activity of Cu/TiO₂ catalysts. I. Influence of the preparation method on the dispersion of copper in Cu/TiO₂, *J. Catal.* 165 (1997) 129–139.
- [17] N. Cristianini, J. Shawe-Taylor, *An Introduction to Support Vector Machines: And Other Kernel-Based Learning Methods*, Cambridge University Press, Cambridge, 2000.
- [18] D.M. Smyth, The role of impurities in insulating transition metal oxides, *Prog. Solid State Chem.* 15 (1984) 145–171.
- [19] B.K. Narayanan, S.A. Akbar, P.K. Dutta, A phosphate-based proton conducting solid electrolyte hydrocarbon gas sensor, *Sens. Actuators B*, in press.
- [20] N.F. Szabo, H. Du, S.A. Akbar, A. Soliman, P.K. Dutta, Microporous zeolite modified yttria stabilized zirconia (YSZ) sensors for nitric oxide (NO) determination in harsh environments, *Sens. Actuators B* 82 (2002) 142–149.